JTTEE5 17:662–670
DOI: 10.1007/s11666-008-9218-9
1059-9630/$19.00 © ASM International

Suspension Plasma-Sprayed Alumina Coating Structures: Operating Parameters Versus Coating Architecture

O. Tingaud, A. Grimaud, A. Denoirjean, G. Montavon, V. Rat, J.F. Coudert, P. Fauchais, and T. Chartier

(Submitted May 8, 2008; in revised form July 21, 2008)

Suspension plasma spraying (SPS) is able to process sub-micrometric-sized feedstock particles and permits the deposition of layers thinner (from 5 to 50 μm) than those resulting from conventional atmospheric plasma spraying (APS). SPS consists in mechanically injecting within the plasma flow a liquid suspension of particles of average diameter varying between 0.02 and 1 μm, average values. Upon penetration within the DC plasma jet, two phenomena occur sequentially: droplet fragmentation and evaporation. Particles are then processed by the plasma flow prior their impact, spreading and solidification upon the surface to be covered. Depending upon the selection of operating parameters, among which plasma power parameters (operating mode, enthalpy, spray distance, etc.), suspension properties (particle size distribution, powder mass percentage, viscosity, etc.), and substrate characteristics (topology, temperature, etc.), different coating architectures can be manufactured, from dense to porous layers. Nevertheless, the coupling between the parameters controlling the coating microstructure and properties are not yet fully identified. The aim of this study is to further understand the influence of parameters controlling the manufacturing mechanisms of SPS alumina coatings, particularly the spray beads influence.

Keywords alumina coating, microstructure, spray bead, suspension plasma spraying

1. Introduction

Suspension plasma spraying (SPS) is an emerging technology and an alternative to atmospheric plasma spraying (APS) to manufacture thinner layers (from 5 to 50 μm, average values) (Ref 1, 2). It consists in axially or radially injecting within a plasma flow a suspension of submicrometer-sized particles. In the present study, mechanical injection has been considered, that is to say that a continuous stream of suspension exiting from an injector of a few tens of micrometers is injected into the plasma flow where it experiences first fragmentation, the resulting droplets encountering then solvent evaporation prior simultaneous acceleration and melting of particles until their impact onto the substrate to be covered (Ref 3, 4).

The main differences between SPS and APS are (Table 1): (i) the carrier gas used to provide micrometric-sized particles with adequate momentum to be injected into the plasma jet in APS that is replaced by a carrier liquid which experiences fragmentation (in a few μs) and vaporization (in a few tens of μs) when interacting with the plasma jet; (ii) the stand-off distance which is shorter in SPS (~40 mm) compared to APS (~100-140 mm) due to the lower thermal and kinetic inertia of submicrometric particles; (iii) a higher heat flux transferred from the plasma to the substrate that can reach values as high as 25 MW m^{-2} in some cases (Ref 5).

In SPS, the liquid stream or drops penetrate the plasma jet if their densities of momentum are significantly higher than the one of the plasma (since upon penetration, the size of the drops decreases due to solvent vaporization). Upon penetration within the plasma flow, the liquid stream encounters two mechanisms, fragmentation and vaporization (Ref 6). In a first approximation and whatever the droplet characteristic dimension, the vaporization duration is two orders of magnitude longer than the fragmentation one. Indeed, the fragmentation occurs for a liquid flow characteristic dimensionless Weber number, *We*, higher than 12-14 (Ref 7). *We* represents the ratio of inertia forces to surface tension forces and is expressed as follows:

$$We = \frac{\rho_{liquid} \Delta V^2 d_{liquid}}{\sigma_{liquid}} \text{(dimensionless)} \qquad \text{(Eq 1)}$$

where ρ_{liquid} is the liquid (suspension) specific mass (kg m^{-3}), d_{liquid} the liquid (suspension) stream

This article is an invited paper selected from presentations at the 2008 International Thermal Spray Conference and has been expanded from the original presentation. It is simultaneously published in *Thermal Spray Crossing Borders, Proceedings of the 2008 International Thermal Spray Conference*, Maastricht, The Netherlands, June 2-4, 2008, Basil R. Marple, Margaret M. Hyland, Yuk-Chiu Lau, Chang-Jiu Li, Rogerio S. Lima, and Ghislain Montavon, Ed., ASM International, Materials Park, OH, 2008.

O. Tingaud, A. Grimaud, A. Denoirjean, G. Montavon, V. Rat, J.F. Coudert, P. Fauchais, and **T. Chartier**, SPCTS-UMR CNRS 6638, Faculty of Sciences, University of Limoges, 123 Avenue Albert Thomas, 87060 Limoges Cedex, France. Contact e-mail: ghislain.montavon@unilim.fr.

Table 1 Major differences between APS and SPS processes

Characteristics	APS	SPS
Particle average size, μm	20-50	0.02-1.0
Particle relative mass, –	1	1.10^{-9}–1.10^{-3}
Feedstock carrier	Gas (Ar usually)	Liquid (H_2O or Et-OH) + additives
Particle mass flow rate, g min^{-1}	20-50	0.75-6
Stand-off distance, mm	100-140	30-50
Heat flux at stand-off distance, MW m^{-2}	2-0.5	25-10

characteristic dimension (m), σ_{liquid} the liquid (suspension) surface tension (considered at ambient temperature in contact with air at ambient pressure) (N m^{-1}), and ΔV is the difference in velocities between the liquid (suspension) stream and the plasma flow (m s^{-1}). The Weber number evolves along the penetration of the suspension within the plasma jet and can reach values as high as 350, leading to a catastrophic break-up (Ref 8).

One can envisage the following simplified sequences for the processing of a suspension made of micrometric-sized particles (Ref 9): (i) fragmentation of the liquid stream occurred before solvent evaporates (two orders of magnitude); (ii) solvent evaporation leads to the formation of single particles or aggregates constituted by a few grains; (iii) these particles melt and form liquid drops which impact, spread, and solidify to form flattened lamellae of equivalent diameters between a few hundred nanometers to a few micrometers.

Lamellae resulting from impact, spreading, and solidification onto the substrate of impinging particles are characterized, apart from their typical size, by (i) almost the absence of peripheral projections around the lamellae; this signifies that the dimensionless flattening Sommerfeld number, K_f, is lower than 6 (Ref 10); and (ii) the absence of intralamellar cracks within the lamellae, *a contrario* to lamellae collected under conventional plasma spray conditions, indicating that the residual quenching stress developing within the lamellae upon rapid solidification and cooling is lower than the intrinsic mechanical resistance of their constitutive material.

The layer results from the stacking of such lamellae and exhibits hence a typical granular structure. Indeed, SPS layers are made of lamellae (molten particles, W), angular particles (unmolten particles, U), and small spherical grains (molten particles resolidified prior their impact upon the substrate, R) (Fig. 1).

This very typical architecture results from several effects/mechanisms:

1. SPS is particularly sensitive to the arc voltage fluctuations induced by the arc instabilities. These voltage fluctuations (Fig. 2) depend upon the plasma torch operating mode (Ref 11, 12), namely the take over mode that develops when the plasma torch is operated with monoatomic plasma forming gases (Ar, He) and characterized by a relative voltage fluctuation, $\Delta V/V$, lower than 0.3 or the restrike mode that develops when the plasma torch is operated with diatomic plasma forming gases (N_2, H_2) and for which $\Delta V/V \geq 1$. The frequency at which the torch voltage fluctuates is about a few kHz, typically from 3 to 5. The available energy in the plasma flow fluctuates together with the voltage fluctuations. The plasma flow average velocity is fluctuating together with the available energy so that the different steps in suspension processing (liquid fragmentation, solvent vaporization, and solid particles melting and acceleration) are not achieved at the same rates all along the time of flight of the feedstock (Ref 13, 14). Indeed, the variations in velocity of the plasma flow, together with its variations in length and position, lead to different locations of the fragmentation of the liquid stream due to the variations in shearing stresses (consecutive to the variation in the plasma momentum density, ρv^2). Moreover, the plasma flow is characterized by strong thermal and kinetic radial gradients (Ref 15)

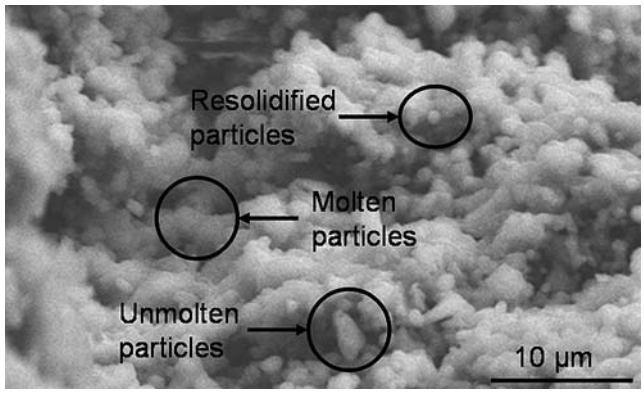

Fig. 1 Typical Al_2O_3 SPS layer architecture (feedstock d_{50} = 500 nm, solvent: Et-OH, particle mass load in suspension MP = 20%, mechanical suspension injection, Ar-H_2 45-15 slpm plasma forming gases, plasma arc current intensity I = 500 A, torch internal nozzle diameter Ø = 5 mm, plasma mass enthalpy h = 14 MJ kg^{-1})

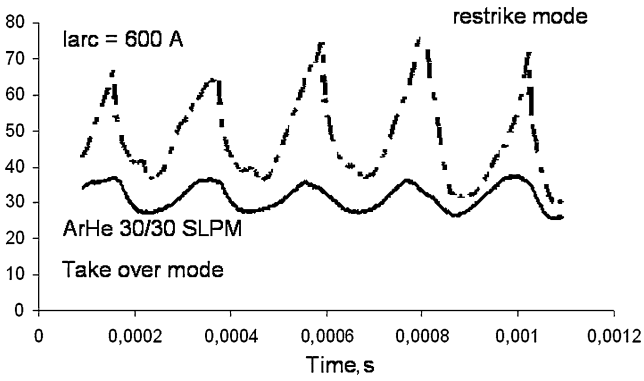

Fig. 2 Arc voltage temporal fluctuations of a DC plasma torch operated under the restrike (Ar-H_2, 45-15 slpm) and the take-over (Ar-He, 30-30 slpm) modes (arc current intensity I = 600 A, anode internal diameter at exit Ø = 5 mm)

providing a heterogeneous energetic transfer from the plasma flow to the droplets and later on to the particles.

2. If the particle size distribution of the solid particles in the suspension is fairly large, this leads to very different characteristic times in the particles processing (Ref 16).
3. In interaction with the plasma jet, the suspension jet crumbles. The first droplets, containing solid particles, fragment from the suspension jet and remain in the plasma fringe, whereas the jet continues its trajectory toward the plasma core (Ref 17). Since the plasma jet is characterized by sharp thermal and kinetic radial gradients (Ref 18, 19), this leads to an inhomogeneous treatment of particles along their trajectories. The solid particles that penetrated into the plasma core will impact upon the substrate in a molten state and form splats, whereas those traveling in the plasma fringes of lower temperature will remain untreated and form angular embedded particles. Spherical particles originate from particles that have been entrained deep into the plasma jet core where they were fully molten before being resolidified either due to the lumped mass heat transfer showing an exponential decrease evolution as a function of the particle diameter (the smaller the particle, the higher the cooling rate) or due to the thermophoresis and related effects (Ref 20) when crossing high thermal gradient regions between the core and the developed jet. Those particles could be hence ejected again in the fringes where they re-solidified due to their low thermal inertia. Even at very short spray distance (30 mm), some spherical grains are embedded within the coating structure. One could consider nevertheless that at such a short spray distance, those particles remain in region of the flow warm enough to not induce solidification. This is why one can estimate that thermophoresis and related effects are not negligible. Nevertheless, at the 50-mm spray distance, the relative fraction of small spherical particles is increased compared to the 30 mm one. One can state hence that a synergy takes place in these conditions between the thermophoresis and the lumped mass heat transfer.

Hence, depending on their size and trajectories, the particles experience different thermal histories and trajectories, leading to different molten state and impact location onto the substrate. Depending upon the fraction of poorly treated particles (processed or re-solidified in the plasma jet core fringes) to the one of appropriately treated (processed in the plasma core and in a molten state when impacting), the coating architecture will evolve from fairly dense (low fraction of poorly treated) to fairly porous (high fraction of poorly treated) (Fig. 3). Densifying the layer architecture requires hence reducing the fraction of poorly treated particles.

Apart from this mechanism, layer architecture depends also upon the manner successive spray beads overlap (Ref 21, 22). Indeed, coating is build up by overlapping the successive spray beads to form the spray pattern. The geometry of the spray bead can be approximated by a Gaussian function that size and shape depend upon the deviation and dispersion of the particle stream at the spray distance (depending themselves upon the plasma power and feedstock injection parameters), the particle state upon impact and plasma torch scan velocity (Ref 21). For fixed spray bead size and shape, the overlapping depends upon the lateral plasma torch scanning step. This is why apart from the optimization of the injection of the suspension and its processing by the plasma flow, the study of spray pattern influences also directly the microstructure of the resulting layer and is hence important to understand the coating formation and to optimize the operating parameters (Ref 23).

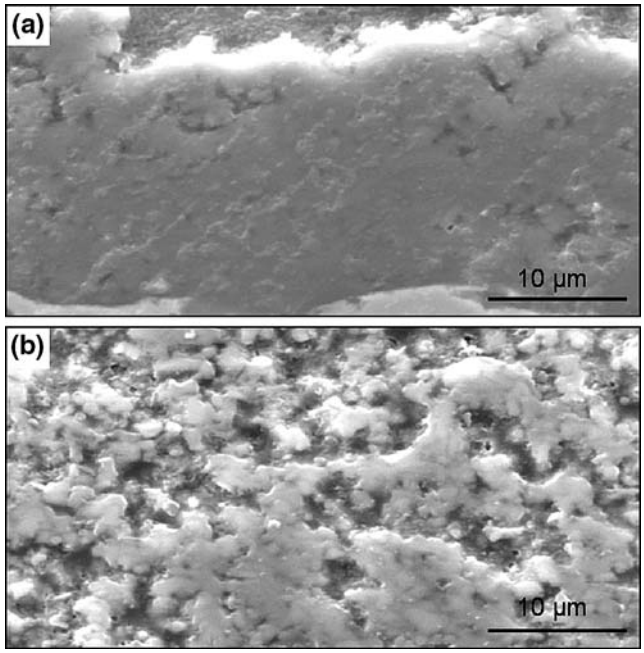

Fig. 3 Typical Al_2O_3 SPS layer architectures manufactured with (a) a low fraction of poorly treated particles (spray distance: 30 mm) and (b) a high one (spray distance: 50 mm) (feedstock $d_{50} = 500$ nm, solvent: Et-OH, MP = 20%, mechanical suspension injection, Ar-H_2 45-15 slpm, $I = 500$ A, $\varnothing = 5$ mm, $h = 14$ MJ kg^{-1})

The aim of this study is hence to assess in particular the effects of spray bead geometry and overlapping on coating structure in view of densifying to the maximum possible extend SPS Al_2O_3 layers. For reference power, suspension, and injection parameters, the spray distance, the number of passes, the spray velocity, and the lateral scanning step were varied to manufacture either spray patterns or layers.

2. Experimental Set-ups

2.1 Operating Parameters and Substrates

A stick-cathode DC plasma torch developed at SPCTS equipped with a 5-mm nozzle internal diameter was used to carry out experiments. It was operated with a binary

Ar-He (30-30 slpm) plasma forming gas mixture and with an arc current intensity of 600 A resulting in a plasma flow mass enthalpy of 12 MJ kg^{-1}. The injection system was composed of a diaphragm with a calibrated hole (150 μm, average diameter). The suspension to be sprayed was stored into a pressurized tank. Depending on the compressed air pressure applied in the tank, the velocity of the suspension at the injector exit varied between 18 and 25 m s^{-1} (momentum density of 0.40 and 0.56 MPa, respectively). The suspension of alumina was made of α-Al_2O_3 P152 SB (Alcan, Saint-Jean de Maurienne, France) of 0.5 μm average diameter (d_{50}), with different mass percentages, MP, of 5, 10, and 20%, respectively, into pure ethanol. To manufacture spray beads and layers, the injection has been optimized to have a penetration of the suspension deep into the plasma flow core. The plasma torch scan velocity (SV) was varied between 0.5 and 1.5 m s^{-1}. The spray distance (SD) was varied from 30 to 50 mm. The substrate temperatures during spraying were estimated using a monochromatic infrared pyrometer (5 μm wavelength). The emissivity was constant during the spray run (whereas it varies with the temperature) and fixed to 0.7. The integration area of the radiation emitted by the substrates was corresponding to surface of equivalent diameter of about 18 mm. Meanwhile such a control does not permit an accurate monitoring of the temperature during spraying; it permits nevertheless to estimate the substrate preheating average temperature to be around 250 °C and the coating average temperature during manufacturing to be about 500 °C.

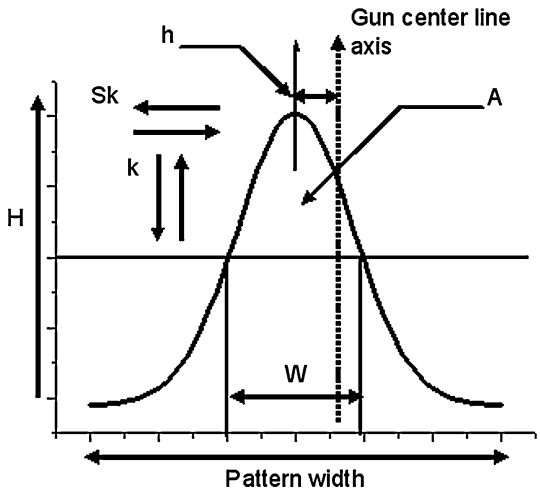

Fig. 4 Spray bead size and shape descriptors

Spray beads were sprayed onto 316L stainless steel plates (120 × 50 × 5 mm) that were previously degreased by immersion in acetone vapors and pre-polished using SiC papers and polished using diamond slurries to obtain different average roughnesses ranging from 0.06 to 0.20 μm. In this case, the plasma torch was moved back and forth in front of the substrates without scanning step.

Coatings were sprayed onto 316L stainless steel buttons (25 mm in diameter and 20 mm in thickness) exhibiting similar average roughnesses. The scanning step (SS) was varied in this configuration from 10 to 20 mm per pass, corresponding to velocities ranging from 0.025 to 0.05 m s^{-1}.

2.2 Measurement of Profiles of Spray Beads

The spray bead profile and its surface average roughness were assessed using a diamond stylus profilometer (Dektak IIA surface profilometer, Sloan Technology, Santa Barbara, USA). Ten measurements randomly located along the bead were carried out on each sample. After adjustment (by discarding the highest and the lowest values), data were averaged. Gaussian functions were selected to fit, with correlation factors ranging from 0.95 to 0.99, the bead profiles. Additional size and shape factors were defined (Fig. 4) such as (Ref 24): (i) the spray bead cross-sectional area A (mm^2) representative of the intrinsic deposition efficiency, the spray bead width L (mm), its maximal height H (μm), its width at half-height W (mm), the mean value m (dimensionless) of the Gaussian distribution, see Eq 2, and its standard deviation σ (dimensionless), see Eq 3; (ii) the spray bead offset h (mm) from the gun centerline axis and the scattering angle α (°) representing the dispersion cone angle of deposited materials (tan α = SD/L); (iii) the pattern skewness Sk (dimensionless), see Eq 4, representing the third moment of the height distribution profile and quantifying the asymmetry of the profile height distribution; and (iv) the spray pattern kurtosis k (dimensionless), see Eq 5, representing the fourth order moment of the height distribution profile and quantifying the flatness/sharpness of the profile height distribution.

Table 2 Profile deposit beads characteristics for different operating conditions

	Sample	H, μm	L, mm	W, mm	A, mm^2	α, °	m, −	Sk, −	k, −	R_a, μm	R_z, μm
NP (−) (for SD = 30 or 40 mm, MP = 10% and SV = 1 ms^{-1})	76(30 mm)	18.20	13.30	4.48	0.112	23.9	5.81	0.98	−0.54	0.80	5.16
	38(30 mm)	7.85	13.70	5.25	0.052	24.5	2.90	0.33	−1.22	0.42	3.36
	152(30 mm)	53.00	18.48	6.64	0.441	31.6	17.81	0.04	−1.13	2.14	8.25
	76(40 mm)	16.10	16.60	6.70	0.135	22.5	6.12	0.16	−1.27	1.17	6.53
	38(40 mm)	6.10	15.00	5.49	0.046	20.5	2.28	0.88	−0.88	0.51	4.11
	152(40 mm)	58.50	17.40	7.47	0.548	23.5	21.93	0.03	−1.37	2.90	10.56
SV (m s^{-1}) (for NP = 75, SD = 40 mm, MP = 10%)	1.5	10.20	12.80	4.80	0.065	17.7	3.86	0.96	−0.85	0.86	5.86
	0.5	17.40	21.50	9.07	0.187	28.3	6.95	0.39	−1.42	1.11	6.71
MP (%) (for NP = 75, SV = 1 ms^{-1}, SD = 40 mm)	5	28.80	21.50	8.08	0.292	28.2	10.08	0.72	−1.18	1.49	10.93
	20	24.50	20.50	8.44	0.260	27.1	9.53	0.56	−1.36	1.32	6.90

$$m = \frac{1}{L}\int_0^L z\,dx \quad \text{(Eq 2)}$$

$$\sigma = \sqrt{\frac{\int_0^L (z-m)^2\,dx}{L}} \quad \text{(Eq 3)}$$

$$Sk = \int_0^L \frac{(z-m)^3\,dx}{\sigma^3 L} \quad \text{(Eq 4)}$$

$$k = \int_0^L \frac{(z-m)^4\,dx}{\sigma^4 L} \quad \text{(Eq 5)}$$

where $z(x)$ is the pattern height function (μm) that represents the local probability density function of the particle impact distribution onto the substrate.

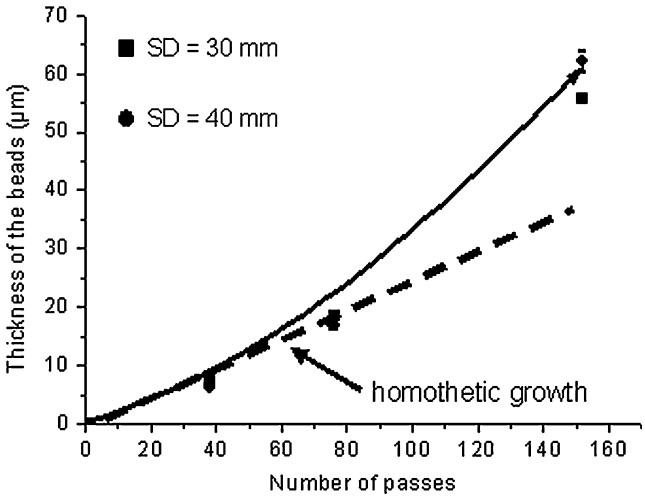

Fig. 5 Evolution of the bead thickness versus the number of passes

Moreover, two characteristics were evaluated in order to define the surface roughness. The average roughness, R_a (μm), that is the arithmetic mean of the absolute heights of roughness profile on the assessment length and the average maximum peak-to-valley height of the roughness profile within the sampling length, R_z (μm). The measurements were made parallel to the spray pattern (with a cut-off of 0.8 mm). All the profile characteristic measurements are listed in Table 2.

Cross sections and top of views of spray pattern and coating architectures were observed by secondary electron-scanning electron microscopy (SE-SEM).

3. Results and Discussion

3.1 Effect of the Number of Passes

At moderated numbers of passes (NP), the spray bead exhibits a homothetic evolution corresponding to a linearly growth of the deposited material (Fig. 5) that disappears then at higher numbers of passes. This can be explained as follows. When the number of passes increases, i.e., when the time spraying increases, the temperature of the sample increases too, up to 500 °C. The smaller particles (<1 μm) can stick at such temperature to the deposited beads (Ref 25) generating stacking defects between two successive passes. One could consider also that the increase in surface roughness of the bead could also form preferential impact locations for impinging particles.

This denotes that for a high number of passes the cohesion between the particles/lamellae decreases and so the surface irregularities and the layer porosity increase (Fig. 6). The average thickness deposited per pass can be hence estimated as varying from 0.20 to 0.25 μm per pass (for MP = 10% and SD = 30 mm).

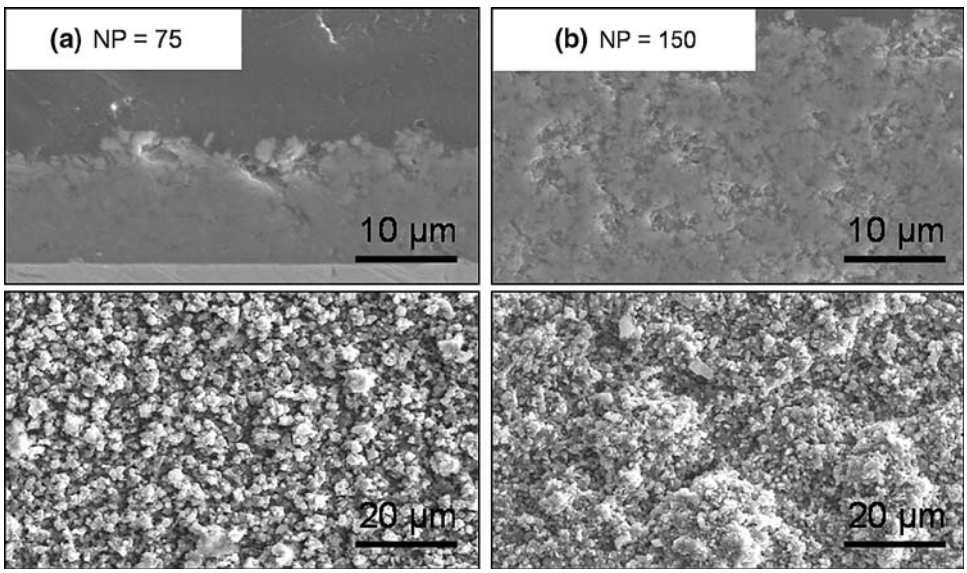

Fig. 6 Al_2O_3 SPS deposited bead architectures and surface topologies for two values of number of passes

3.2 Effect of the Spray Distance

The height and area of the spray beads present a quadratic evolution as a function of the spray distance (Fig. 7). This evolution is analogous to the one of the intrinsic deposition efficiency versus the spray distance. The highest values correspond to SD = 30 mm (average deposited thickness per pass higher than 0.20 µm), whereas they very significantly decrease to almost 0 for SD = 50 mm, demonstrating the criticity of the spray distance in the SPS process. Moreover, as the spray distance increases, the fraction of poorly treated particles is increased (mostly due to the low thermal inertia of particles) and the resulting coating architecture and surface topology are affected, being more porous and irregular (Fig. 8).

3.3 Effect of the Spray Velocity

In a first approximation, the spray bead size and shape criteria evolve linearly with an increase in the plasma torch scan velocity, SV, as shown in Fig. 9, which depicts the evolutions of the normalized bead area, *A*, width at half-height, *H*, and the scattering angle, α, versus the spray velocity. Those criteria decrease when SV increases. Indeed, the poorly treated particles generate stacking defects and hence promote porous and heterogeneous architectures (Fig. 10). At low velocity, those particles are better removed from the coating and the high heat flux transferred from the plasma to the substrate can keep locally the successive impinging particles in a molten state, or close to it, leading to denser coatings.

3.4 Effect of the Powder Mass Load

The powder mass percentage in suspension seems to influence directly the dispersion and deviation angles of the sprayed material. Indeed, the spray pattern characteristics do not present a continuous evolution but show an

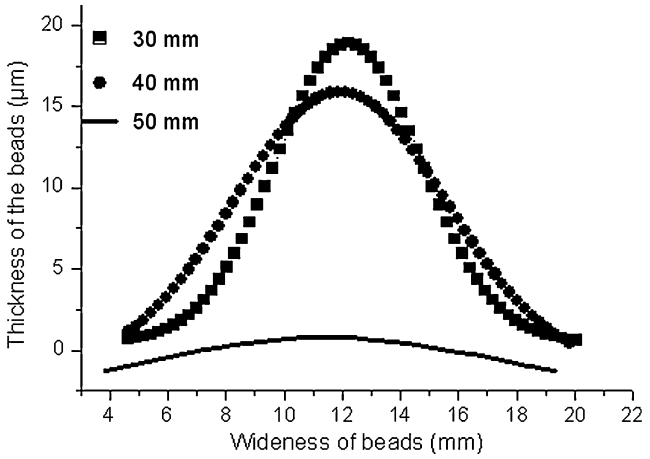

Fig. 7 Bead profiles manufactured at different spray distances

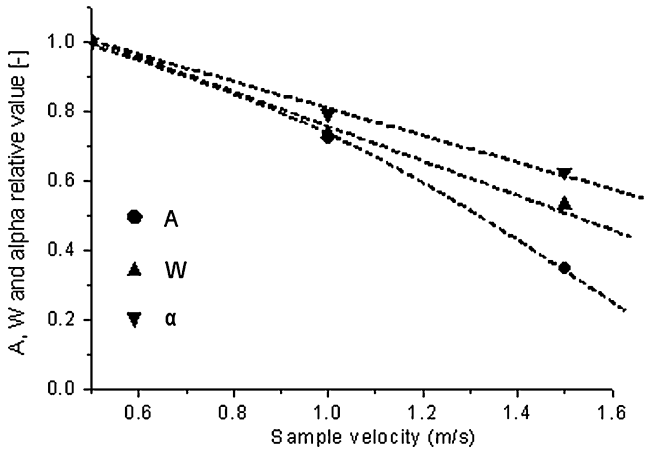

Fig. 9 Deposit profiles versus spray velocity

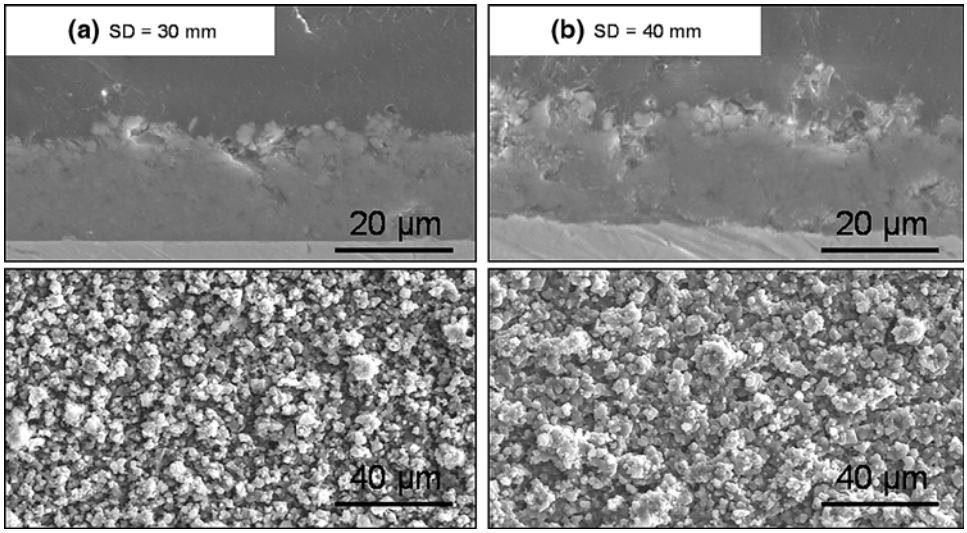

Fig. 8 Al_2O_3 SPS deposited bead architectures and surface morphologies at different spray distances

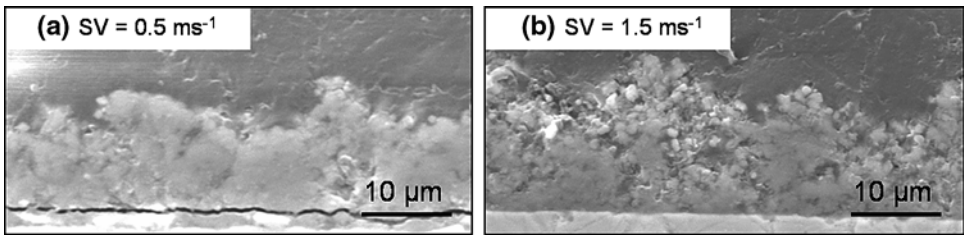

Fig. 10 Al_2O_3 SPS deposited bead architectures for different spray velocities

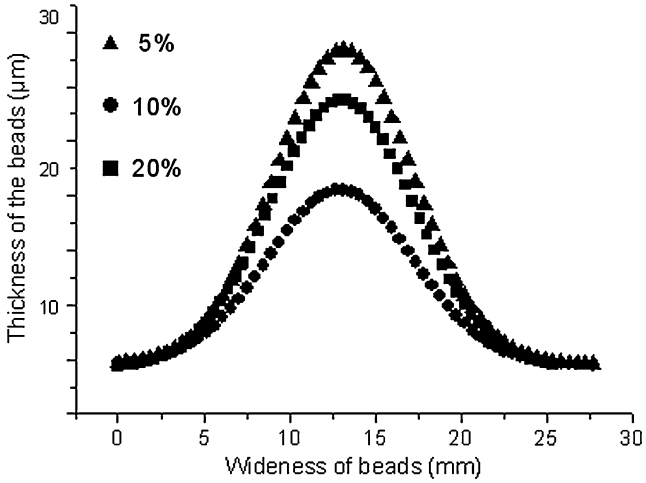

Fig. 11 Evolution of the spray bead profiles versus the powder mass percentage in suspension

extremum for MP = 10% (Fig. 11). At such a value, the dispersion angle is lowered, leading to a better treatment of the particles in the plasma jet. Therefore, the fraction of poorly treated particles is decreased and the coating density is increased consequently (Fig. 12). *A contrario*, for MP = 5 or 20%, the dispersion is increased and the fraction of poorly treated particles embedded into the spray bead is increased, leading to a porous coating architecture. MP becomes critical at high values (higher than 20%) and causes the layer delamination very likely due to the too high fraction of poorly treated particles embedded within the structure.

3.5 Comparison Between the Structures of Spray Beads and Coatings

The aforementioned results permit to clearly define some trends to adjust operating parameters to manufacture coatings with various pore levels.

At short spray distances (30-40 mm) and low powder mass percentage (5-10%), coatings are denser than those manufactured at longer spray distances (50 mm) or higher mass load (20%) (Fig. 13). By estimating the quantity of poorly treated particles embedded in the coating P (resolidified R and unmolten U particles) to the quantity of well melted particles M (molten particles), a qualitative ratio T = P/M can be defined as a function of operating parameters (plasma torch scan velocity, number of passes, spray distance, etc.).The higher the ratio, the higher the density of stacking defects and so the higher the pore level.

Moreover, the coatings manufactured at SD = 50 mm are very heterogeneous and porous whatever the other operating parameters, clearly demonstrating the criticity of the spraying distance on the coating microstructure. At last, for MP = 20%, the layers are porous and very poorly cohesive (some are even fractured). This is mostly due to the thermal stresses which develop during deposition consecutively to the high rate of poorly treated particles embedded into the coatings. Those particles are not removed by successive passes of the plasma torch in front of the substrate surface and consequently this generates a high density of stacking defects.

3.6 Temperature During Coating Manufacturing

During coating manufacturing, the average substrate temperature has been estimated to be about 500 °C. Even if the heat flux transmitted by the plasma flow to the substrate is fairly high at such short spray distance (a few MW m^{-2}), in situ sintering should not occur due to the too low temperature and relatively short duration at this temperature.

Nevertheless, temperature reaches very likely locally much higher values particularly at a 30-mm spray distance. Under such conditions, fast sintering mechanism could be achieved. Works are underway to identify such phenomena and to quantify them.

4. Conclusion

Several operating parameters including the spray distance, the number of passes, the spray velocity, and the powder mass percentage in suspension were varied to discriminate their effects upon sizes, shapes, and structures of spray patterns and structures of coatings.

The deposit shape and microstructure evolution have been linked to different operating conditions and have permitted to optimize the kinematics parameters to obtain dense or porous coating in a better reproducible way. The growth law and the average thickness deposited per pass have been quantified. The plasma torch scan velocity and

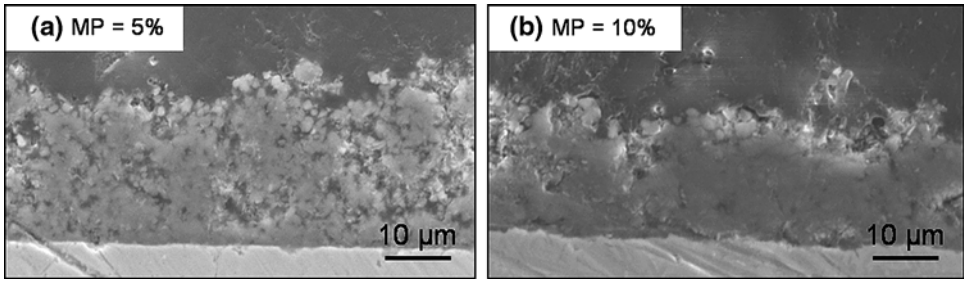

Fig. 12 Al_2O_3 SPS deposited bead architectures at different powder mass percentages in suspension

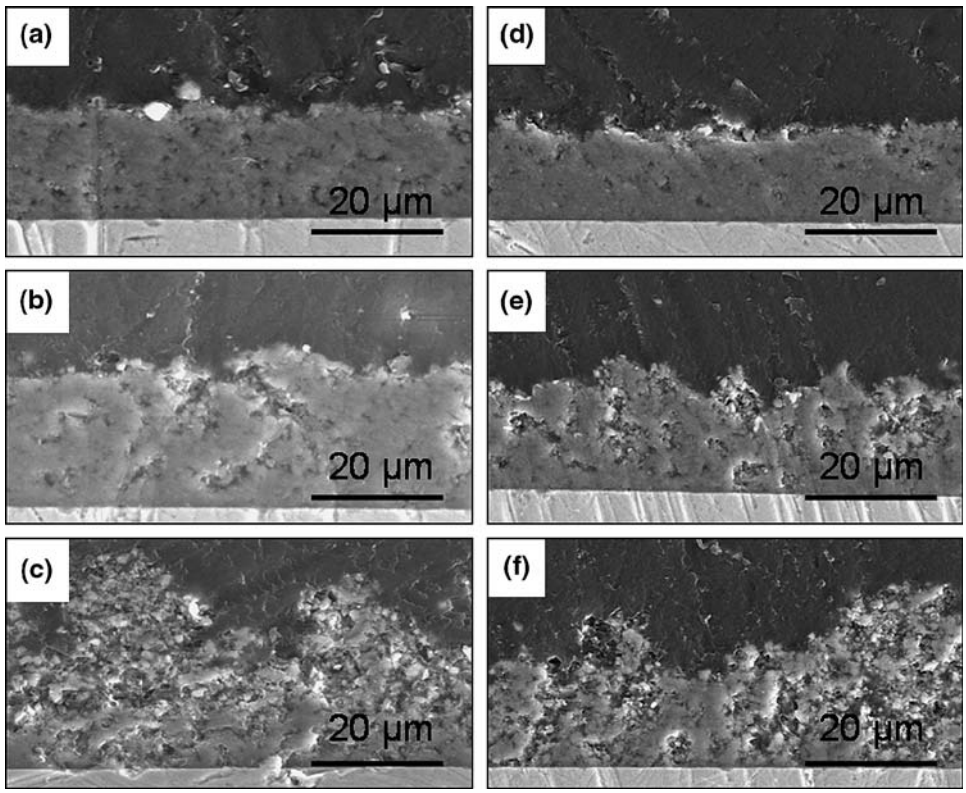

Fig. 13 Al_2O_3 SPS coating microstructures for MP = 5% at (a) 30 mm, (b) 40 mm, and (c) 50 mm, and for MP = 10% at (d) 30 mm, (e) 40 mm, and (f) 50 mm

especially the spray distance affect the microstructure of the coating and the deposition efficiency. An increase in those parameters leads to an increase in the pore level and a decrease in the layer cohesion. The powder mass load also plays a role but its effects are of lower amplitude.

This study demonstrates that besides the criticity of the fragmentation processes that are related to the processing of the liquid stream by the plasma jet bringing together the suspension properties, the injection configuration and the plasma flow thermodynamic properties, the kinematics and geometric parameters including the spray distance and the torch scan velocity and scanning step, are also very important in SPS process and permit to control the coating architecture.

References

1. R. Siegert, J.E. Döring, J.L. Marqués, R. Vaβen, D. Sebold, and D. Stöver, Denser Ceramic Coatings Obtained by the Optimization of the Suspension Plasma Spraying Technique, *Thermal Spray Solutions – Advances in Technology and Application*, DVS-Verlag GmbH, Düsseldorf, Germany, 2005, ISBN: 3-87155-792-7
2. R. Rampon, C. Filiatre, and G. Bertrand, Suspension Plasma Spraying of YPSZ Coatings for SOFC: Suspension Atomization and Injection, *J. Therm. Spray Technol.*, 2008, **17**(1), p 105-114
3. J. Jaworski, L. Pawlowski, F. Rondet, S. Kozerski, and A.L. Magner, Influence of Suspension Plasma Spraying Process Parameter on TiO_2 Coatings Microstructure, *J. Therm. Spray Technol.*, 2008, **17**(1), p 73-81
4. S. Bouaricha, J. Oberste-Berghaus, J.G. Legoux, C. Moreau, and T. Chraska, Suspension Plasma Spraying of Nano-Ceramics Using an Axial Injection Torch, *Thermal Spray Connects:*

Explore its Surfacing Potential!, E. Lugscheider, Ed., DVS-Verlag GmbH, Düsseldorf, Germany, 2005, ISBN: 3-87155-793-5
5. R. Etchart-Salas, ''Atmospheric Plasma Spraying of Submicron-Sized Solid Particles in Suspension. Experimental and Analytical Approach of Involved Phenomena in Reproducibility and Quality of Coatings,'' Ph.D. Thesis, University of Limoges, France, 2007 (in French)
6. B.E. Gelfand, Droplet Breakup Phenomena in Flows with Velocity Lag, *Prog. Energy Combust. Sci.*, 1996, **22**, p 201-265
7. T. Watunabe and K. Ebihara, Numerical Simulation of Coalescence and Breakup of Rising Droplets, *Comput. Fluids*, 2003, **32**, p 823-834
8. C.S. Lee and R.D. Reitz, Effect of Liquid Properties on the Breakup Mechanism of High Speed Liquid Drops, *Atomization Sprays*, 2001, **11**, p 1-19
9. J. Fazilleau, C. Delbos, V. Rat, J.-F. Coudert, P. Fauchais, and B. Pateyron, Phenomena Involved in Suspension Plasma Spraying Part 1: Suspension Injection and Behavior, *Plasma Chem. Plasma Proc.*, 2006, **26**(4), p 371-391
10. P. Fauchais, M. Fukumoto, A. Vardelle, and M. Vardelle, Knowledge Concerning Splat Formation: An Invited Review, *J. Therm. Spray Technol.*, 2004, **13**(3), p 337-360
11. M.P. Planche, J.F. Coudert, and P. Fauchais, Velocity Measurements for Arc Jets Produced by d.c. Plasma Spray Torches, *Plasma Chem. Plasma Proc.*, 1998, **18**, p 263-283
12. J. Oberste-Berghaus, J.-G. Legoux, and C. Moreau, Injection Conditions and In-Flight Particle States in Suspension Plasma Spraying of Aluminia and Zirconia Nano-Ceramics, *Thermal Spray Connects: Explore its Surfacing Potential!*, E. Lugscheider, Ed., DVS-Verlag GmbH, Düsseldorf, Germany, 2005, ISBN: 3-87155-793-5
13. J.-F. Bisson and C. Moreau, Effect of Direct-Current Plasma Fluctuations on In-Flight Particle Parameters: Part II, *J. Therm. Spray Technol.*, 2003, **12**, p 256-265
14. R. Etchart-Salas, V. Rat, J.-F. Coudert, and P. Fauchais, *Thermal Spray 2007: Global Coating Solutions*, B.R. Marple, M.M. Hyland, Y.-C. Lau, C.-J. Li, R.S. Lima, and G. Montavon, Eds., CD-Rom, Pub. ASM International, Materials Park, OH, USA, 2007, ISBN: 0-87170-809-4
15. P. Fauchais, Understanding Plasma Spraying, *J. Phys. D: Appl. Phys.*, 2004, **37**, p R86-R108
16. C. Delbos, ''Contribution to the Understanding of Ceramic (Y-PSZ, Perovskite, etc.) or Metallic (Ni, etc.) Particles Injection by a Liquid Carrier in a Plasma Jet to Manufacture Finely-Structured Coatings for SOFC,'' Ph.D. Thesis, University of Limoges, 2004 (in French)
17. O. Tingaud, A. Grimaud, A. Denoirjean, G. Montavon, V. Rat, J.-F. Coudert, and P. Fauchais, Effects of Operating Parameters on SPS Alumina Coatings Structures to Manufacture Functionally-Graded Layers, *Surf. Coat. Technol*. (in press)
18. Y.P. Wan, J.R. Fincke, S. Sampath, V. Prasad, and H. Herman, Modeling and Experimental Observation of Evaporation from Oxidizing Molybdenum Particles Entrained in a Thermal Plasma Jet, *Int. J. Heat Mass Transf.*, 2002, **45**, p 1007-1015
19. I. Ahmed and T.L. Bergman, Three-Dimensional Simulation of Thermal Plasma Spraying of Partially Molten Ceramic Agglomerates, *J. Therm. Spray Technol.*, 2000, **9**, p 215-224
20. X. Chen, Heat and Momentum Transfer Between a Thermal Plasma and Suspended Particles for Different Knudsen Numbers, *Thin Solid Films*, 1999, **345**(1), p 140-145
21. L. Xie, X. Ma, A. Ozturk, E.H. Jordan, N.P. Padture, B.M. Cetegen, D.T. Xiao, and M. Gell, Processing Parameter Effects on Solution Precursor Plasma Spray Process Spray Patterns, *Surf. Coat. Technol.*, 2004, **183**(1), p 51-61
22. F.-I. Trifa, G. Montavon, and C. Coddet, Model-Based Expert System for Design and Simulation of APS Coatings, *J. Therm. Spray Technol.*, 2007, **16**(3), p 128-139
23. E. Pfender, Thermal Plasma Technology: Where do We Stand and Where are We Going?, *Plasma Chem. Plasma Proc.*, 1999, **19**, p 1-31
24. F.-I. Trifa, G. Montavon, and C. Coddet, On the Relationships Between the Geometric Processing Parameters of APS and the Al_2O_3-TiO_2 Deposit Shapes, *Surf. Coat. Technol.*, 2005, **195**, p 54-69
25. A. Haddadi, R. Hamacha, A. Grimaud, P. Fauchais, and F. Nardou, Residual Stresses and Microstructure of Plasma Sprayed Zirconia Coatings, *High Temp. Mater. Processes*, 1998, **2**(3), p 327-337